Dalton Transactions

Synthesis and Characterization of Rhodium-Aluminum Heterobimetallic Complexes Tethered by a 1,3-Bis(diphenylphosphino)-2-propanoxy Group

Journal:	*Dalton Transactions*
Manuscript ID	DT-ART-03-2019-000938.R1
Article Type:	Paper
Date Submitted by the Author:	26-Apr-2019
Complete List of Authors:	Li, Zhongjing; University of Memphis, Chemistry Yokley, Timothy; University of Memphis, Chemistry Tran, Sheila; University of Memphis, Chemistry Zong, Jie; Pennsylvania State University, Chemistry Schley, Nathan; Vanderbilt University, Chemistry Brewster, Timothy; University of Memphis, Chemistry

Synthesis and Characterization of Rhodium-Aluminum Heterobimetallic Complexes Tethered by a 1,3-Bis(diphenylphosphino)-2-propanoxy Group

Zhongjing Li,[†] Timothy W. Yokley,[†] Sheila L. Tran,[†] Jie Zong,[‡] Nathan D. Schley,[⊥] Timothy P. Brewster[*,†]*

[†] Department of Chemistry, The University of Memphis, 3744 Walker Avenue, Smith Chemistry Building, Memphis, Tennessee 38152, United States

[‡] Department of Chemistry, The Pennsylvania State University, University Park, PA 16802 United States

[⊥] Department of Chemistry, Vanderbilt University, Nashville, Tennessee 37235, United States

Abstract We demonstrate the synthesis and characterization of a new class of late transition metal-aluminum heterobimetallic complexes. A bridging ligand which both chelates the transition metal and binds the aluminum via an alkoxide was employed to impart stability to the bimetallic system. Novel rhodium-aluminum heterobimetallic complexes Rh(DPPE)(DPPP-O-Al^{i}Bu$_2$Cl) and Rh(DPPP-O-Al^{i}Bu$_2$)(DPPP-O-Al^{i}Bu$_2$Cl) are synthesized and spectroscopically characterized.

INTRODUCTION

Heterobimetallic complexes have gained intense attention due to their interesting structures, properties, and applications such as in theranostics,[1] medical imaging,[2] and catalysis.[3,4] In particular, early-late heterobimetallic complexes have been widely explored.[5-7] The large polarity difference between metal centers make them nicely suitable for cooperative heterolytic bond activations.[8,9] In a similar fashion, as the most electropositive element in group 13, a highly Lewis acidic aluminum(III) center would be expected to impart significant polarity into a late transition metal heterobimetallic system.

Aluminum-containing heterobimetallics are rare in comparison to early/late transition metal systems and when compared to analogous complexes containing its less acidic Group 13 congener, boron.[10-15] The scarcity of aluminum heterobimetallic complexes is largely due to the challenging synthesis. Successful syntheses typically require careful ligand design to buttress Al to the late transition metal. For example, representative complexes developed by Lu feature a *hepta*- dentate ligand that cages Al and the transition metal to facilitate formation of a Z-Type bond.[15-19] Lu's aluminum complexes have been found capable of N_2 activation,[15] with gallium analogues able to activate and transfer hydrogen.[17] One catalysis drawback of these systems is the limited access of substrate to the Lewis acidic site. Aluminum is completely caged by the ligand, thereby relegated to inductively adjusting the electronic properties of the metal center – it cannot participate cooperatively in catalysis without ligand dissociation.

Bourissou[20] and Emslie[21] developed alternative, sterically accessible systems by employing geometrically constrained phosphine-alane ligands. The complexes obtained by Bourissou cooperatively activated bonds in CO_2, CS_2, H_2, and $PhCONH_2$, though no catalysis was reported. In Emslie's systems, a 1,1'-bis(phosphino)ferrocene ligand was employed to facilitate formation of a Pt-Al bond. In the first catalytically useful example of a Z-type late metal-aluminum heterobimetallic system, Iwasawa employed a terpyridine pincer ligand with two coordinating phosphorus arms to cage Pd and Al.[22] The resulting complexes are effective for hydrosilylation of CO_2. Later, a Ni/Al complex reported by Nakao was found to facilitate C-H functionalization of pyridines.[23] Interestingly, a formal metal-aluminum bond is not required for cooperative catalysis to occur, merely proximity of the two sites. For example, hydrocarbamoylation of alkenes was achieved in a bridged Ni/Al system reported by Cramer.[24] The limited number of well characterized examples of late metal-aluminum heterobimetallics, combined with their

recently demonstrated catalytic utility, makes the development of new heterobimetallic constructs an area ripe for exploration.

Our laboratory has been exploring the synthesis of Ir-Al and Rh-Al heterobimetallic complexes, with the aim of exploiting these two metal centers for cooperative activation of small molecules in a manner reminiscent of a Frustrated Lewis Pair.[25-27] A "transition metal first" synthetic strategy in which the reactive aluminum center is added to the bimetallic species following the synthesis of the transition metal component was developed to overcome the inherent synthetic difficulty of working with moisture sensitive compounds.[28] In recent experiments, a proof-of-concept result has been obtained demonstrating that the heterobimetallic Ir-Al and Rh-Al complexes developed in our laboratory can facilitate the activation of small molecules.[29]

We now report the synthesis and characterization of a new series of Rh-Al heterobimetallic complexes. In our initial paper,[28] we reported a slow, thermal decomposition of the rhodium-containing heterobimetallic complexes. Analysis of a decomposition product informed us that dissociation of the bridging pyridone ligand from rhodium was responsible for the observed decomposition. To alleviate this concern we envisioned replacing the pyridine moiety with a chelating phosphine ligand. In the work reported below, 1,3-bis(diphenylphosphino)-2-propanol (DPPP-OH)[30] has been utilized to tether rhodium and aluminum. As in our previous work, to ensure stable attachment of the aluminum motif, it will be linked to a bridging ligand through a thermodynamically strong Al-O bond.

RESULTS AND DISSCUSSION

Synthesis The general synthesis procedures are summarized in Scheme 1 (for further information, see Experimental Details). The overall strategy is similar to our reported

procedure,[28] where aluminum was introduced at the end of the reaction sequence by reacting tri-isobutyl aluminum (Al^iBu_3) with an aluminum-binding hydroxyl group on pre-assembled transition metal complexes, thereby taking advantage of the easy formation of aluminum-oxygen bonds and eliminating the need to further manipulate air- and moisture-sensitive aluminum compounds.

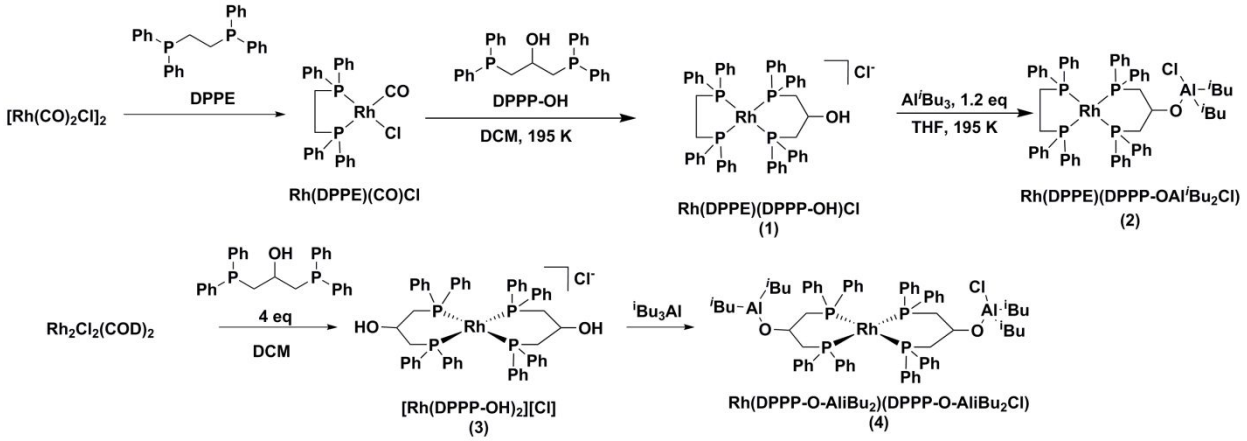

Scheme 1. Synthetic procedure for Rh(DPPE)(DPPP-O-Al^{i}Bu$_2$Cl) and Rh(DPPP-O-Al^{i}Bu$_2$)(DPPP-O-Al^{i}Bu$_2$Cl)

In the synthesis of Rh(DPPE)(DPPP-OH)Cl (**1**), the assembly was designed to install DPPE and DPPP-OH sequentially on to rhodium from readily accessible $Rh_2(CO)_4Cl_2$.[31] The reaction conditions were empirically optimized and carefully controlled to avoid unintentional formation of $[Rh(DPPE)_2]^+$, $[Rh(DPPP\text{-}OH)_2]^+$, DPPP-OH bridged dimers,[32] or other species. First, Rh(DPPE)(CO)Cl was obtained by reacting DPPE with $Rh_2(CO)_4Cl_2$.[31] The $^{31}P\{^1H\}$ NMR spectrum of Rh(DPPE)(CO)Cl showed two sets of *dd* peaks that are characteristic of Rh-P and P-P splitting (see Figure S3 in the Supporting Information). Further treatment of Rh(DPPE)(CO)Cl with DPPP-OH resulted in the formation of **1**. The $^{31}P\{^1H\}$ NMR spectrum of **1** displayed a diagnostic, two signal pattern for the two phosphorus in DPPE and the two phosphorus in DPPP-OH respectively, as shown in Figure S6 in the Supporting Information. The two phosphorus centers in each DPPE or DPPP are chemically equivalent (δ 19.68 ppm and 16.78 ppm,

respectively) but magnetically inequivalent, leading to an AA'BB'X spin system wherein each phosphorus atom is coupled to the other three and the $I = ½$ rhodium center.

The observed $^{31}P\{^{1}H\}$ coupling patterns within **1** are second-order as a result of the coupling between two nuclei with identical chemical shifts [$^{2}J_{P\text{-}P}$ >>>> 10*(Δδ)]. Thus, the coupling constants cannot be extracted by simply using peak spacing and relative peak intensity. However, the pattern can be effectively modeled based on parameterized chemical shift and coupling constants, as shown in Figure 1 below, allowing for full coupling analysis. As is often observed in highly second-order spin systems, the sign of the coupling constant *J* has a remarkable effect on the observed pattern. In this system, *cis* $^{2}J_{P\text{-}P}$ coupling constants were found to be negative (parallel spins lower in energy) while the *trans* $^{2}J_{P\text{-}P}$ coupling constants were positive (opposite spins lower in energy). Measurement of negative $^{2}J_{P\text{-}P}$ values is not uncommon in bis-phosphine systems.[33]

Treatment of **1** with Al^{i}Bu$_3$ resulted in the target heterobimetallic complex Rh(DPPE)(DPPP-O-Al^{i}Bu$_2$Cl) (**2**). Unfortunately, the well-known complex [Rh(DPPE)$_2$]Cl[34,35] was formed as a byproduct during the synthesis of **2**. The two complexes are not easily separated, and the bis-DPPE impurity is present as a minor component in our product spectra (see Figure S7 in Supporting Information). After extensive recrystallization, the mole percentage of [Rh(DPPE)$_2$]Cl could be reduced to below 5% (calculated from integration of the $^{31}P\{^{1}H\}$ NMR spectrum of the product mixture). The $^{31}P\{^{1}H\}$ NMR spectrum of **2** displayed a similar, diagnostic, coupling pattern to that observed in **1**. Aluminum coordination causes the second order multiplet for the DP*P*P-O-Al^{i}Bu$_2$Cl phosphorus resonance to shift slightly upfield to δ 13.90 ppm from the resonance observed in the parent complex (δ 16.78 ppm, see Figure 2). The DP*P*E resonance remains largely unchanged at δ 59.37 ppm. Full coupling constant information

for this AA'BB'X system can be found in the Experimental Details and in the Supporting Information.

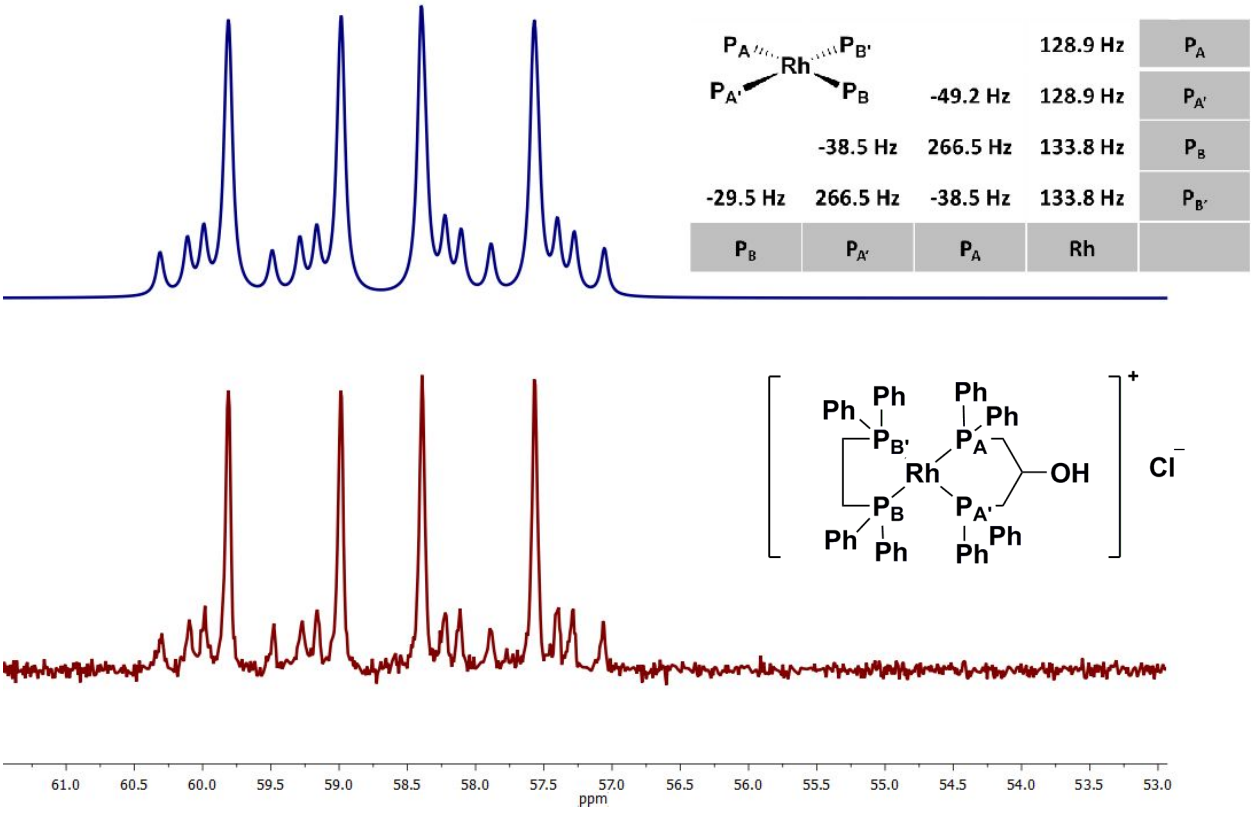

Figure 1. Modeled (blue, above) and experimental (red, below) fine pattern of the $^{31}P\{^{1}H\}$ NMR spectrum for the two phosphorus atoms in the DPPE ligand (P_B, P_B' in table) in complex **1**. An analogous peak is found for the DPPP-OH ligand. Inset: P-P and Rh-P coupling constants; P_A, $P_{A'}$ (DP***P***P-OH), P_B, $P_{B'}$ (DP***P***E). For full spectrum, see Figure S3 in the Supporting Information.

The ^{1}H NMR spectrum of **2** also contains three critical diagnostic features that unambiguously confirm our assignment of the structure of the major reaction product. First, the integration of the signals corresponding to alane protons clearly indicated the loss of one equivalent of its alkane substituent. Second, the remaining methylene protons between δ 0.65 and 0.75 are now diasterotopic, coupled to each other with a geminal coupling constant of 13.6 Hz. This strongly indicates successful docking to the alkoxide *and* the formation of a tetrahedral of aluminum center via chloride coordination. Third, the signal arising from the methine protons

shifted downfield due to steric deshielding[36] after reaction between $^{i}Bu_3Al$ and the hydroxyl group on DPPP-OH. These phenomena are consistent with nitrate-bound aluminum centers in the heterobimetallic complexes previously described in our laboratory.[28] The ^{1}H NMR spectrum was modeled using simple, first-order coupling parameters to obtain the relevant coupling information (as shown in Figure 3). Full coupling parameters can be found in the Experimental Details.

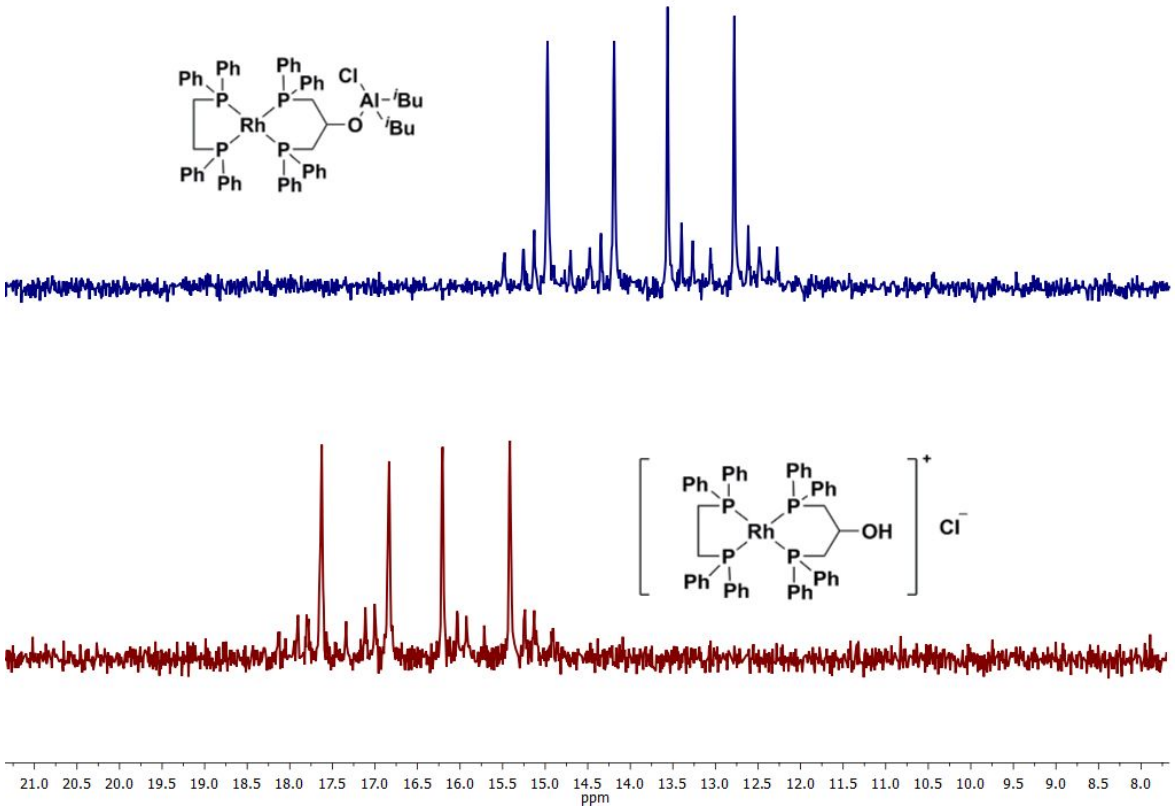

Figure 2. Truncated $^{31}P\{^{1}H\}$ NMR spectrum of **2** showing the shift in the DP*P*P-O-R resonance on moving from R = H (bottom) to R = Al($^{i}Bu_2$)Cl (top).

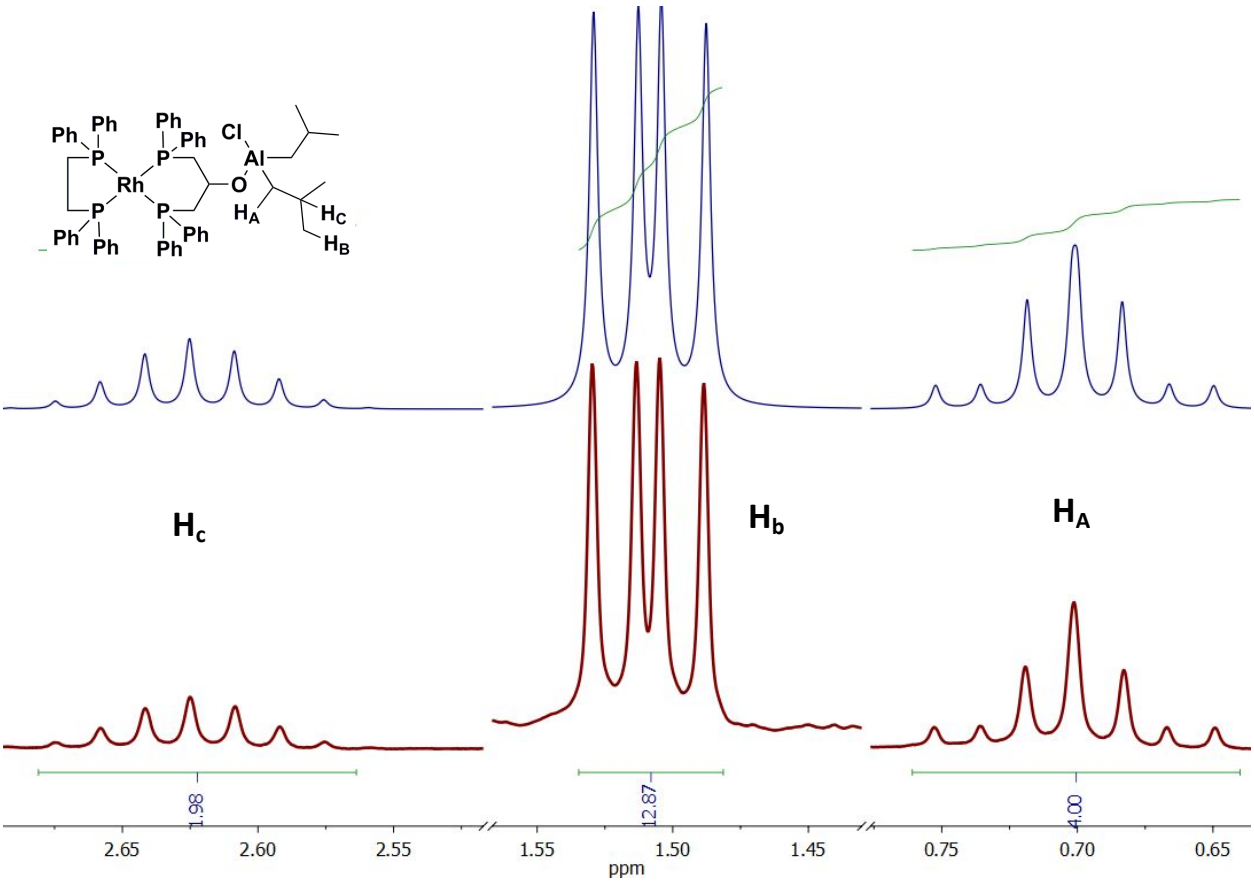

Figure 3. Modeled (top) and measured (bottom) ^{1}H NMR spectrum of aluminum alkyl resonances in **2**.

In an effort to eliminate the formation of unwanted inseparable byproducts, we then shifted our attention to the synthesis of a new target complex, Rh(DPPP-O-Al^{i}Bu$_2$)(DPPP-O-Al^{i}Bu$_2$Cl) (**4**), where we replaced the troublesome DPPE ligand with a second equivalent of DPPP-OH. The precursor, [Rh(DPPP-OH)$_2$]Cl (**3**), was synthesized in a straightforward manner by treating $Rh_2(COD)_2Cl_2$[31] with 4.2 equivalents of DPPP-OH followed by washing COD and excess DPPP-OH away with a mixed solvent system of pentane/dichloromethane (v/v = 5/1). Though we were unable to obtain X-ray quality crystals of the chloride complex, anion metathesis with Na(BArF$_{24}$) in dichloromethane (BArF$_{24}$ = tetrakis(3,5-trifluoromethylphenyl)borate) followed by slow precipitation from a solution of [Rh(DPPP-OH)$_2$][BArF$_{24}$] (**3-BArF**) in chloroform

layered with pentane did yield suitable crystals of the $BArF_{24}$ analogue (Figure 4). The complex is found to have a distorted square planar geometry, with *cis* P-Rh-P angles of 88.51° and 88.18° within the metallacycles and 98.33° and 98.67° between the metallacyles (sum of angles = 373.69°). The two hydroxide functionalities also are located in equatorial positions of their respective pseudo-chair metallacycles and are found to be mutually *cis* within the spiro ring system. Interestingly, the deviation from planarity observed in the solid state structure of **3-BArF** is not observed in the solid state structure of $[Rh(DPPP)_2][Cl]$[37] (DPPP = diphenylphosphinopropane, structure found in Figure 4, sum of angles = 360.1°) suggesting that the steric demand of the hydroxyl group has a measurable impact on the observed structural metrics.

Interestingly, the synthesis of **3** from $[Rh(CO)_2Cl]_2$ was not successful. CO dissociation from Rh was found to be incomplete, leading to the formation of the penta-coordinate complex $[Rh(DPPP\text{-}OH)_2(CO)]Cl$ (**5**). An X-ray crystal structure of this unexpected product was obtained by layering a chloroform solution of the complex with pentane (Figure 5). Complex **5** displays a trigonal bipyramidal structure (sum of equatorial angles = 360.1°, P_{axial}-Rh-P_{axial} = 173.76°) with the carbonyl ligand occupying one of the equatorial positions. As in the structure of **3-BArF** above, the two hydroxide functionalities also are located in equatorial positions of their respective pseudo-chair metallacycles and are found to be mutually *cis* within the spiro ring system.

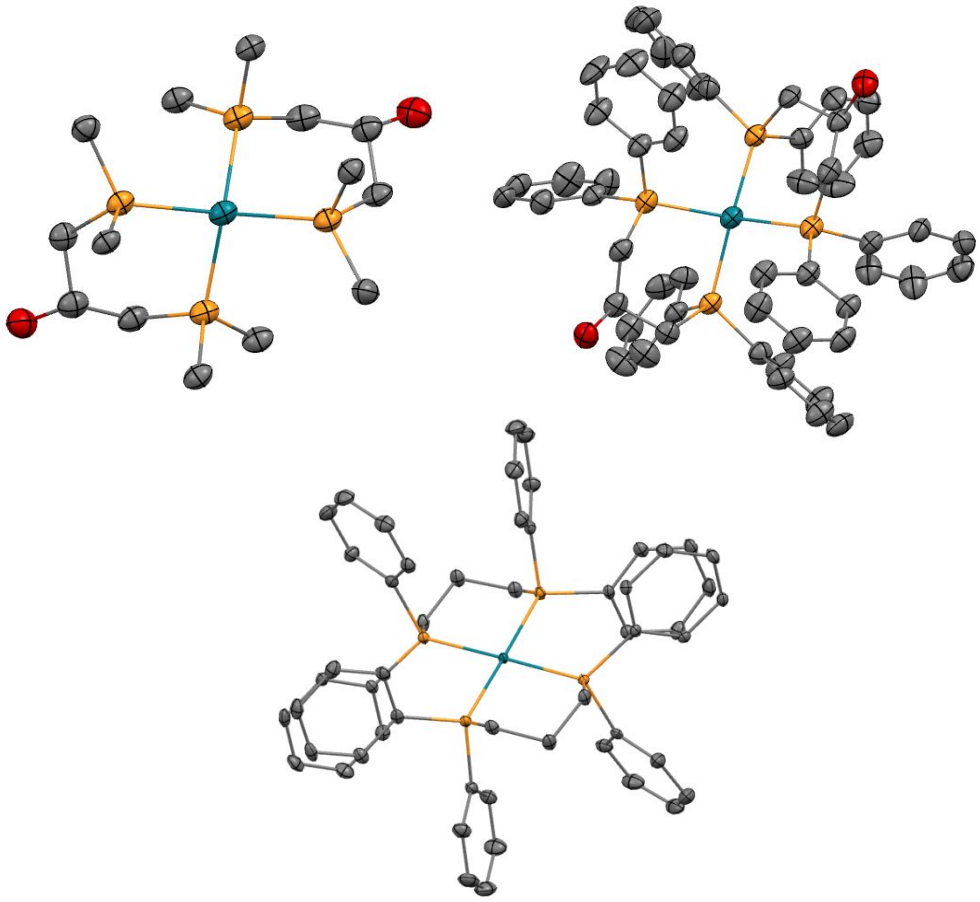

Figure 4. Top: ORTEP representations of **3-BArF**. Left: Carbons 2-6 of each phenyl ring omitted for clarity. Right: Full structure. Bottom: ORTEP representation of [Rh(DPPP)][Cl]. For all structures, ellipsoids shown at 50% probability. Hydrogen atoms and anion omitted from each structure for clarity.

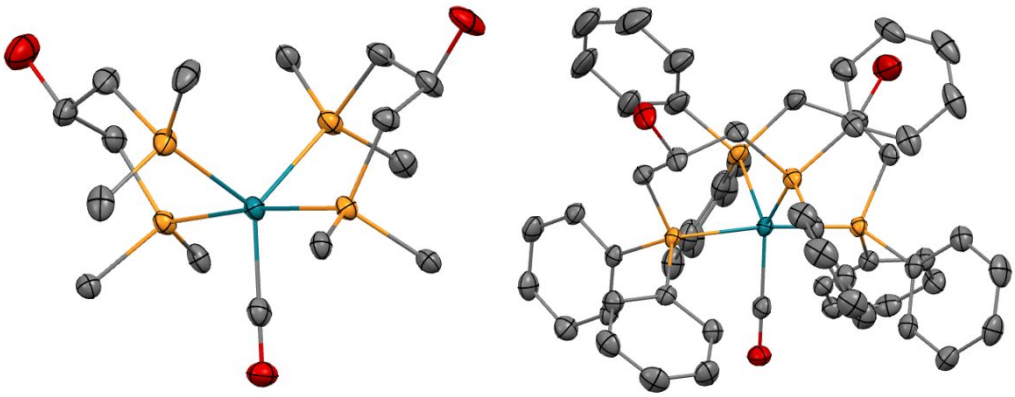

Figure 5. ORTEP representations of **5**. Ellipsoids shown at 50% probability. Hydrogen atoms and chloride counterion omitted for clarity. Left: Carbons 2-6 of each phenyl ring omitted for clarity. Right: Full structure.

Treatment of **3** with Al^iBu_3 resulted in the target heterobimetallic complex Rh(DPPP-O-Al^iBu_2)(DPPP-O-Al^iBu_2Cl) (**4**). Unfortunately, solid-state characterization of **4** has not been possible due to its dynamic nature and its intrinsically high reactivity. The ^1H NMR spectrum (Figure S12) is quite broad, but features a number of upfield ($\delta < 0.5$ ppm) resonances consistent with the presence of the aluminum alkyl. The $^{31}P\{^1H\}$ NMR spectrum of **4** at room temperature features a sharp doublet and a broad secondary feature (as shown in Figure S11, Supporting Information). Variable temperature NMR in dichloromethane-d_2 was carried out to further elucidate the observed broadness of the $^{31}P\{^1H\}$ spectrum, as shown in Figure 6, below.

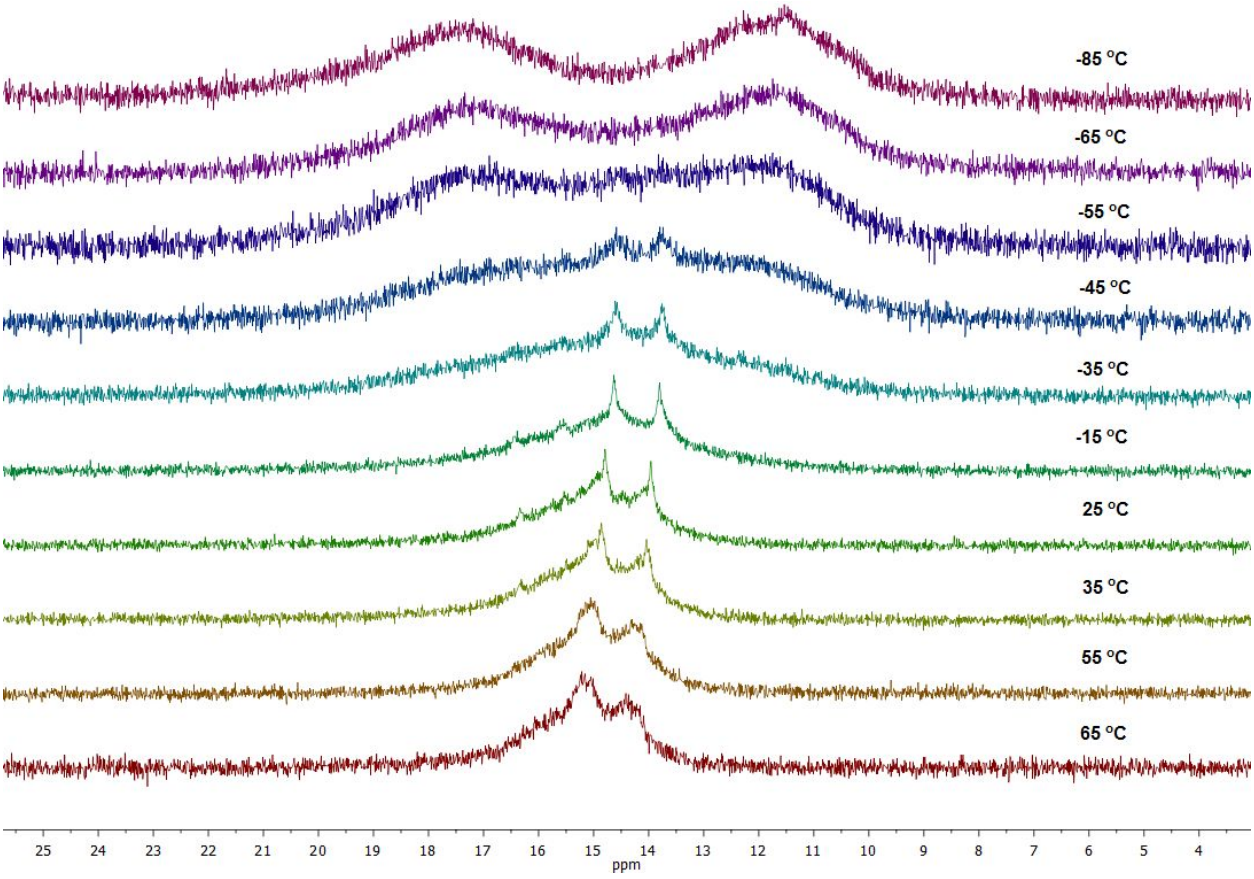

Figure 6. Variable temperature $^{31}P\{^1H\}$ NMR of **4**. Temperature recorded across a range from -85°C to 65°C.

Two processes were observed as temperature changes. The first process is evident at very low temperature. Two broad peaks (~ δ 17.44 and δ 11.72 ppm) with clear separation could be

observed at -85°C via $^{31}P\{^{1}H\}$ NMR spectroscopy. As the temperature is raised, these two peaks began to broaden and shift with coalescence observed at approximately -15°C. In the second dynamic process, a doublet with a coupling constant of 133 ppm, first observable at -55°C, first sharpens significantly with rising temperature. Above room temperature, this signal begins to broaden slightly and shift downfield. Though we were unable to increase the temperature above 65°C on our NMR spectrometer, it appears that the broad, underlying feature begins to coalesce with the sharp doublet at high temperature. The distinction between the two features is evident in the room temperature spectrum shown in Figure S11 (Supporting Information). Importantly, signals arising from the precursor complex **3** are not observed in the product spectrum suggesting that the observed behavior is intrinsic to the reaction product mixture, **4**.

Though the exact nature of the dynamic species in solution has not yet been rigorously established, we have significant evidence that the formulaic assignment of complex **4** is correct. First, ESI-MS (Figures S13 and S14 in Supporting Information) of **4** under different ionization conditions showed different patterns that could be assigned as fragments arising from **4**. Under all ionization conditions, a peak at 960.08 from precursor $[Rh(DPPP\text{-}OH)_2]^+$ (*m/z* = 960) was seen suggesting the Al-O bond as a likely fragmentation location (the starting material was not observed by NMR spectroscopy). Higher-mass fragments assignable to [Rh(DPPP-O-Al^{i}Bu)(DPPP-O-Al^{i}Bu)•H_2O]$^+$ (*m/z* = 1144, water arises from injection port contamination) and [Rh(DPPP-O-Al^{i}Bu$_2$)(DPPP-O-Al^{i}Bu$_2$)]$^+$ (*m/z* = 1240) were also easily identified, confirming that aluminum has docked successfully. High Resolution Mass Spectrometry provided further validation for the formation of the desired product (Fig S15, Supporting Information). At no point in any ESI-MS experiment were mass fragments greater than the parent ion of **4** observed, strongly suggesting that **4** is monomeric, rather than dimeric or oligomeric, in solution.

Further support for a monomeric product was obtained from DOSY (Figures S18 and S19). Complexes in the product mixture **4** all diffuse at the same rate, indicating a uniform product size. Importantly, they also diffuse at the same rate as complex **3**, which is known to be monomeric from the solid state structure of **3-BArF**. This suggests that **3** and **4** are of similar size. Were **4** dimeric or oligomeric, it would be expected to diffuse much more slowly than **3**.

With this knowledge in hand, we propose a reasonable explanation for the dynamic behavior observed in the NMR spectra of **4**. We first postulate that the two distinct fluxional processes derive from two different, isomeric products. This is consistent with complex **3** which exists as a mixture of *cis* and *trans* isomers (Figure 7). It is quite likely, given the low temperature of the synthesis of **4** from **3** that interconversion between the *cis* and *trans* forms is not possible during synthesis. Thus, observing two distinct species with distinct dynamic behavior is not unexpected. At high temperatures, where dissociative interconversion may become feasible, the two species would be expected to interchange. This is consistent with the observed high temperature broadening in Figure 6. Notably, any dissociative pathways available above room temperature could also facilitate intramolecular scrambling of DPPP-O-Al^{i}Bu$_2$ ligands with DPPP-O-Al^{i}Bu$_2$Cl ligands further contributing to line broadening and complicating the analysis of the high-temperature spectra. We favor dissociative (as opposed to associative) ligand exchange as a mechanism due to precedent[38,39] and the steric bulk of the phosphines.

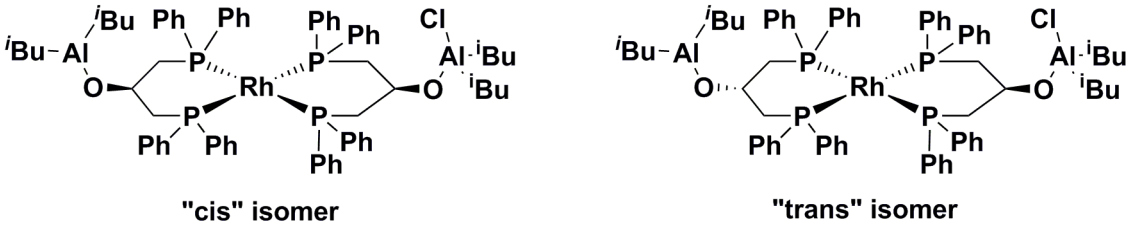

Figure 7. Possible diastereomers of **4**.

Additionally, we postulate that the dynamic behavior observed for each isomer relates to chloride exchange between the aluminum centers. As can be clearly seen in Figure 7, the two DPPP-O-Al ligands in **4** should be chemically inequivalent, as one contains a bound chloride and the other does not. One would, thus, expect an AA'BB'X coupling pattern in the phosphorus NMR as was observed for complexes **1** and **2**. What is instead observed at room temperature is a sharp doublet, indicating that all four phosphorus centers are equivalent (via exchange). The most likely explanation for this is chloride scrambling. The different molecular geometries of the *cis* and *trans* isomers would cause differential activation barriers to exchange, thus resulting in their unique dynamic behavior.

Though we believe that our explanation above is the most plausible given the data in hand, other possibilities for dynamic behavior exists. First, each diastereomer could undergo slow chair-chair interconversion. Given the significant preference for the bulky O-Al^{i}Bu to occupy an equatorial position off the six-membered metallacycle, we believe that this is unlikely to be observed. Other potential dynamic behavior derives from the aluminum center itself. To maintain charge balance, at least one aluminum must be coordinatively unsaturated. It could then engage in a multitude of potential stabilizing interactions. First, it could dimerize via a bridging alkyl with a neighboring aluminum center. We consider this possibility unlikely due to the steric bulk of the isobutyl group (Al^{i}Bu$_3$ does not exist as a dimer), the DPPP-O ligand, and the lack of evidence for dimer formation by ESI-MS and DOSY. The aluminum center could also engage in weak, intramolecular, Z-type bonding with the transition metal center. However, to attain such a geometry, the 6-membered metallacycle would be forced to adopt a boat geometry, which is likely energetically unfavorable even with a stabilizing Z-type bond.

Finally, we attempted to extend the synthetic protocols utilized here to other aluminum moieties. Interestingly, no other commercially available aluminum alkyls led to the formation of readily identifiable heterobimetallics. $AlEt_3$, $AlEt_2Cl$, and Al^iBu_2Cl, all facilitated transformation of the Rh precursors into a mixture of intractable products. The unique reactivity of Al^iBu_3 is attributed to the bulky size of isobutyl groups, which provide efficient steric protection of the Al center. Chloride, which in addition to its small steric profile can readily bridge between two aluminum centers, further complicates syntheses from $AlEt_2Cl$, and Al^iPr_2Cl.

CONCLUSIONS

Highly polarized heterobimetallic complexes are a promising catalyst family for the cooperative activation of polarizable substrates. In an effort to overcome the instability of the pyridone bridge in previously reported late transition metal-aluminum complexes from our laboratory[28] and prevent decomposition in the presence of a substrate, a synthetic route to a novel heterobimetallic complex, **2**, which is bridged via a ligand which chelates the transition metal was developed. Thorough spectroscopic characterization indicated the presence of a small amount of $[Rh(DPPE)_2]Cl$ in the product mixture. The thermodynamic stability of this undesired byproduct led us to develop a synthetic route to **4**. This complex was found to have a dynamic structure in solution. Application of these exciting complexes toward small molecule activation is now under investigation.

EXPERIMENTAL SECTION

Procedures were performed in a nitrogen-filled Inert Technologies glovebox or using standard Schlenk techniques unless otherwise specified. Extra dry benzene, pentane, tetrahydrofuran, diethyl ether, and dichloromethane were purchased from commercial suppliers and stored over molecular sieves in the glovebox prior to usage. Toluene was dried over calcium

hydride and stored over molecular sieves in the glovebox. Deuterated solvents were purchased from Cambridge Isotope Laboratories, dried over molecular sieves, and stored in the glovebox prior to use. DPPE was purchased from Sigma-Aldrich. DPPP-OH was synthesized following literature procedure.[30] $NaBArF_{24}$ was synthesized by the method of Bergman[40] and purified using the modification reported by Peters.[41] All other reagents and solvents used were commercially available and used without further purification. Aluminum and phosphine reagents were stored in a nitrogen glovebox prior to use. ^{1}H and ^{13}C NMR spectra were recorded on a 400 MHz JEOL spectrometer and referenced to the residual solvent peak.[42] Additional NMR data were obtained on a 400 MHz JEOL spectrometer and referenced to an appropriate external standard (^{31}P: H_3PO_4 in D_2O (0.00 ppm)). Spectra were modeled using the MestReNova 10 software package. ESI-MS was measured on a ThermoFisher LTQ-XL ion trap mass spectrometer from dichloromethane or tetrahydrofuran solution. High resolution mass spectra were recorded on a Waters Synapt High Resolution Mass Spectrometer housed at the University of Memphis. Elemental analysis was performed by Atlantic Microlabs, Inc. and is reported as the average of duplicate runs.

Rh(DPPE)(CO)Cl This procedure was adapted from the synthetic protocol for the analogous iridium complex.[32] $RhCl_3 \cdot 3H_2O$ (1.37 g, 5 mmol) was dissolved in 100 mL methanol. The mixture was heated to reflux under CO for 24 hours. The bright yellow solution was cooled to room temperature and methanol was removed by vacuum. The dark red solid was dissolved in 50 mL benzene, to which a benzene solution (100 mL) of 1,2-bis(diphenylphosphino)ethane (2.0 g, 5 mmol) was added dropwise. The yellow precipitate was collected and recrystallized from dichloromethane/hexanes, affording 2.3 g yellow powder as product. Yield: 80%. ^{1}H NMR (400 MHz, $CDCl_3$) δ 7.71-7.83 (m, 8 H), 7.40 (m, 12 H), 2.42-2.49 (m, 2 H), 2.15-2.22 (m, 2 H).

$^{31}P\{^{1}H\}$ NMR (162 MHz, $CDCl_3$) δ 71.17 (dd, J =159.6, 34.8 Hz), 49.46 (dd, J = 127.2, 34.8 Hz). Anal. Calc $C_{27}H_{24}OP_2RhCl$: C, 57.42; H, 4.28. Found: C, 57.39; H, 4.40.

Rh(DPPE)(DPPP-OH)Cl (1) To a stirred dichloromethane (5 mL) solution of DPPP-OH (215 mg, 0.5 mmol) at -78 °C, Rh(DPPE)(CO)Cl (280 mg, 0.5 mmol) in dichloromethane (10 mL) was added dropwise over a period of 1 hour. The mixture was allowed to stir for 16 hours as the temperature was slowly raised from -78 °C to room temperature. The crude product was purified by recrystallization from tetrahydrofuran at -35 °C. 370 mg yellow powder was collected as product. Yield: 77%. ^{1}H NMR (400 MHz, Chloroform-d) δ 7.51 (m, 4H), 7.40 – 6.96 (m, 28H), 6.82 (m, 8H), 3.83 (s, 1 H), 3.66-3.69 (m, 1 H), 2.90 (m, 2H), 2.71 (m, 2H), 2.06 (m, 2H), 1.86 (m, 2H). $^{31}P\{^{1}H\}$ NMR (162 MHz, $CDCl_3$) δ 59.68 (DP*P*E, J_{Rh} = 133.8 Hz, J_{trans} = 266.5 Hz, $J_{cis,\ B\text{-}B'}$ = -29.5 Hz, $J_{cis,\ B\text{-}A'}$ = -38.5 Hz), 16.78 (DP*P*P-OH, J_{Rh} = 128.9 Hz, J_{trans} = 266.5 Hz, $J_{cis,\ A\text{-}A'}$ = -49.2 Hz, $J_{cis,\ A\text{-}B'}$ = -38.5 Hz). Anal. Calc $C_{53}H_{50}OP_4RhCl$: C, 65.95; H, 5.22. Found: C, 58.79; H, 5.02. Elemental consistent with two molecules of dichloromethane per formula unit (C, 58.20, H, 4.80).

Rh(DPPE)(DPPP-O-Al^{i}Bu$_2$Cl) (2) To a stirred tetrahydrofuran (3 mL) solution of Rh(DPPE)(DPPP-OH)Cl formed in situ from Rh(DPPE)(CO)Cl (141 mg, 0.25 mmol) and DPPP-OH (110 mg, 0.25 mmol) at -78 °C, $^{i}Bu_3Al$ (50 mg, 0.25 mmol) was added. The mixture was allowed to stir for 1 hour and warmed from -78 °C to room temperature. After the reaction, tetrahydrofuran was removed by vacuum. The resultant yellow powder was dissolved in 0.5 mL tetrahydrofuran and precipitated by the addition pentane. This recrystallization was repeated twice to remove $[Rh(DPPE)_2]Cl$ and improve purity to greater than 95%. 170 mg bright yellow powder was collected as product. Impurity prevented acceptable microanalysis from being obtained. Yield: 62%. ^{1}H NMR (400 MHz, tetrahydrofuran-d_8) δ 6.60 – 7.36 (m, 56H), 5.36 (m,

1 H), 2.91 (m, 2H), 2.74 (m, 2 H), 2.62 (m, 2 H), 1.52 (d, J = 6.6 Hz), 1.50 (d, J = 6.6 Hz), 0.72 (dd, J_{gem} = 13.5 Hz, J = 6.6 Hz), 0.68 (dd, J_{gem} = 13.5 Hz, J = 6.6 Hz). $^{31}P\{^{1}H\}$ NMR (162 MHz, tetrahydrofuran-d_8) δ 59.37 (DP*P*E, J_{Rh} = 107.2 Hz, J_{trans} = 205.5 Hz, $J_{cis,\ B\text{-}B'}$ = -22.6 Hz, $J_{cis,\ B\text{-}A'}$ = -29.2 Hz), 58.20 (Rh(DP*P*E)$_2$Cl, d, J = 132.8 Hz), 13.90 (DP*P*P-OH, *ddd*, J_{Rh} = 101.2 Hz, J_{trans} = 205.5 Hz, $J_{cis\ A\text{-}A'}$ = -39.4 Hz, $J_{cis,\ A\text{-}B'}$ = -29.2 Hz). HRMS calculated for $[C_{53}H_{50}Al_2O_4P_4Rh]^+$ (product of alkyl hydrolysis) m/z calc: 971.1554. Found: 970.8866 (See Figures 17a and 17b in Supporting Information).

[Rh(DPPP-OH)$_2$]Cl (3) To a stirred dichloromethane (5 mL) solution of $Rh_2(COD)_2Cl_2$ (49 mg, 0.1 mmol), DPPP-OH (170 mg, 0.4 mmol) in dichloromethane (5 mL) was added dropwise. The mixture was stirred at room temperature for 30 min before the solution was concentrated by vacuum to ~1 mL. The product was obtained via precipitation with pentane. This recrystallization was repeated twice to yield 122 mg of yellow powder. This product exists as a mixture of two isomers, as determined by $^{31}P\{^{1}H\}$ NMR spectroscopy and confirmed by combustion analysis. Yield: 61%. $^{31}P\{^{1}H\}$ NMR (162 MHz, $CDCl_3$) δ 14.14 (d, J = 134 Hz), 13.39 (d, J = 134 Hz). Anal. Calc $C_{54}H_{52}O_2P_4RhCl$: C, 65.17; H, 5.27. Found: C, 64.88; H, 5.42.

Rh(DPPP-O-Al^{i}Bu$_2$)(DPPP-O-Al^{i}Bu$_2$Cl) (4) To a stirred tetrahydrofuran (3 mL) solution of [Rh(DPPP-OH)$_2$]Cl (50 mg, 0.05 mmol) at -35 °C, ^{i}Bu$_3$Al (22 mg, 0.11 mmol) was added. The solution was stirred for 10 minutes and tetrahydrofuran was removed by vacuum. The remaining solid was washed with cold pentane three times. The ^{1}H NMR spectrum is broadened due to probable isomeric mixture. ^{31}P NMR (162 MHz, tetrahydrofuran-d_8) δ 15.04 (d, J = 134 Hz). ESI-MS: m/z calc. for: $[C_{62}H_{70}Al_2O_3P_4Rh]^+$ ($[M\text{-}Cl]^+$): 1244.00. Found: 1244.17. HRMS for $[C_{54}H_{54}Al_2O_6P_4Rh]^+$ (product of alkyl hydrolysis during injection) m/z calc: 1079.1557. Found: 1079.0964. See Supporting Information for further ESI-MS analysis.

X-Ray Crystallography

A suitable crystal of each sample was selected for analysis and mounted in a polyimide loop. All measurements were made on a Rigaku Oxford Diffraction Supernova Eos CCD with filtered Cu-Kα radiation at a temperature of 100 K. Using Olex2,[43] the structure was solved with the ShelXT structure solution program using Direct Methods and refined with the ShelXL refinement package[44] using Least Squares minimization.

ASSOCIATED CONTENT

Supporting Information

NMR spectra of newly synthesized compounds, mass spectrometry data, and X-ray data are included. The Supporting Information is available free of charge on the RSC Publications website at DOI: [to be inserted by editorial office].

Accession Codes

CCDC 1900599, 1900600, and 1900601 contain the supplementary crystallographic data for this paper. These data can be obtained free of charge via www.ccdc.cam.ac.uk/data_request/cif, or by emailing data_request@ccdc.cam.ac.uk, or by contacting The Cambridge Crystallographic Data Centre, 12 Union Road, Cambridge CB2 1EZ, UK; fax: +44 1223 336033.

AUTHOR INFORMATION

Corresponding Author

*E-mail: tbrwster@memphis.edu.

ORCID

Timothy P. Brewster: 0000-0002-7654-4106

Nathan D. Schley: 0000-0002-1539-6031

Timothy W. Yokley: 0000-0001-8378-4442

Notes

The authors declare no competing financial interest.

ACKNOWLEDGMENTS

This material is based upon work supported by the National Science Foundation under Grant No. CHE-1531466 and a grant from The University of Memphis College of Arts and Sciences Research Grant Fund. This support does not necessarily imply endorsement by the University of Memphis of research conclusions. The authors thank Prof. Nathan J. DeYonker (University of Memphis) and Prof. D. Michael Heinekey (University of Washington) for helpful discussions. Prof. Paul Simone and Mr. Drake Williams (University of Memphis) are thanked for assistance with obtaining HRMS data. Z.L. thanks the University of Memphis College of Arts and Sciences and Department of Chemistry for a Postdoctoral Fellowship.

References

1 V. Fernández-Moreira, and M. Concepción Gimeno, *Chem. Eur. J.*, 2018, **24**, 3345-3353.
2 N. Desbois,S. Pacquelet, A. Dubois, C. Michelin, and C. Gros, *Beilstein J. Org. Chem.*, 2015, **11**, 2202–2208.
3 M. Böhmer, F. Kampert, T. Tan, G. Guisado-Barrios, E. Peris, and F. Hahn, *Organometallics*, 2018, **37**, 4092-4099.
4 B. Wu, M. Bezpalko, B. Foxmana and C. Thomas, *Chem. Sci.*, 2015, **6**, 2044-2049.
5 N. Wheatley and P. Kalck, *Chem. Rev.*, 1999, **99**, 3379−3420.
6 B. Cooper, J. W. Napoline, and C. M. Thomas, *Catalysis Reviews*, 2012, **54**, 1−40.
7 E. Bodio, M. Picquet, and P. Le Gendre, *Homo- and Heterobimetallic Complexes in Catalysis*, 2015, 139−186.
8 H. Zhang, B. Wu, S. L. Marquard, E. D. Litle, D. A. Dickie, M. W. Bezpalko, B. M. Foxman, and C. M. Thomas, *Organometallics*, 2017, **36**, 3498−3507.
9 G. Culcu, D. A. Iovan, J. P. Krogman, M. J. T. Wilding, M. W. Bezpalko, B. M. Foxman, and C. M. Thomas, *J. Am. Chem. Soc.*, 2017, **139**, 9627-9636.
10 A. Amgoune and D. Bourissou, *Chem. Commun.*, 2011, **47**, 859-871.
11 J. S. Anderson, J. Rittle, and J. C. Peters, *Nature*, 2013, **501**, 84-87.
12 M. Sircoglou, S. Bontemps, G. Bouhadir, N. Saffon, K. Miqueu, W. Gu, M. Mercy, C. Chen, B. M. Foxman, L. Maron, O. V. Ozerov, and D. Bourissou, *J. Am. Chem. Soc.*, 2008, **130**, 16729−16738.
13 J. S. Figueroa, J. G. Melnick, and G. Parkin, *Inorg. Chem.*, 2006, **45**, 7056−7058.
14 B. R. Barnett, C. E. Moore, A. L. Rheingold, and J. S. Figueroa, *J. Am. Chem. Soc.*, 2014, **136**, 10262−10265.

15 P. A. Rudd, S. Liu, L. Gagliardi, V. G. Young Jr., and C. C. Lu, *J. Am. Chem. Soc.*, 2011, **133**, 20724-20727.
16 M. V. Vollmer, J. Xie, R. C. Cammarota, V. G. Young Jr., E. Bill, L. Gagliardi, and C. C. Lu, *Angew. Chem. Int. Ed.* 2018, **57**, 7815-7819.
17 R. C. Cammarota and C. C. Lu, *J. Am. Chem. Soc.*, 2015, **137**, 12486-12489
18 J. T. Moore, N. E. Smith, and C. C. Lu, *Dalton Trans.*, 2017, **46**, 5689-5701.
19 J. Ye, R. C. Cammarota, J. Xie, M. V. Vollmer, D. G. Truhlar, C. J. Cramer, C. C. Lu, and L. Gagliardi, *ACS Catal.*, 2018, **8**, 4955-4968.
20 M. Devillard, R. Declercq, E. Nicolas, A. W. Ehlers, J. Backs, N. Saffon-Merceron, G. Bouhadir, J. C. Slootweg, W. Uhl, and D. Bourissou, *J. Am. Chem. Soc.*, 2016, **138**, 4917−4926.
21 B. E. Cowie, F. A. Tsao, and D. J. H. Emslie, *Angew. Chem. Int. Ed.*, 2015, **54**, 2165-2169.
22 J. Takaya and N.Iwasawa, *J. Am. Chem. Soc.*, 2017, **139**, 6074−6077.
23 Y. Nakao, K. S. Kanyiva, and T. Hiyama, *J. Am. Chem. Soc.*, 2008, **130**, 2448-2449
24 P. A. Donets and N. Cramer. *J. Am. Chem. Soc.*, 2013, **135**, 11772−11775
25 D. W. Stephan and G. Erker, *Angew. Chem., Int. Ed.*, 2010, **49**, 46-76.
26 A. J. M. Miller, J. A. Labinger, and J. E. Bercaw, *Organometallics* 2010, **29**, 4499–4516.
27 A. J. M. Miller, J. A. Labinger, and J. E. Bercaw, *J. Am. Chem. Soc.*, 2010, **132**, 3301–3303.
28 T. P. Brewster, T. H. Nguyen, Z. Li, W. T. Eckenhoff, N. D. Schley, and N. J. DeYonker, *Inorg. Chem.*, 2018, **57**, 1148−1157.
29 R. M. Charles III, T. W. Yokley, N.J. DeYonker and T.P. Brewster, 2019, *In Review.*
30 J. Karas, G. Huttner, K. Heinze, P. Rutsch, and L. Zsolnai, *Eur. J. Inorg. Chem.*, 1999, 405-420.
31 J. A. McCleverty and G. Wilkinson, *Inorg. Syn.*, 1966, **8**, 211-214.
32 B. J. Fisher and R. Eisenberg, *Inorg. Chem.*, 1984, **23**, 3216-3222.
33 R.D. Bertrand, F.B. Ogilvie, J.G. Verkade *J. Am. Chem. Soc.* 1970, **92**, 1908-1915.
34 G. Pilloni, M. Vecchi, and M. Martelli, *J. Electroanal. Chem. Interfacial Electrochem.*, 1973, **45**, 483-485.
35 B. K. Teo, A. P. Ginsberg, and K. C. Kalabrese, *J. Am. Chem. Soc.*, 1976, **98**, 3027-3029.
36 J. Zong, J. T. Mague, and R. A. Pascal Jr., *J. Am. Chem. Soc.*, 2013, **135**, 13235-13237.
37 R. Brady, Warren V. Miller, and L. Vaska, *J. Chem. Soc., Chem. Commun.*, 1974, 393-394.
38 J. Halpern, and C. S. Wong, *J. Chem. Soc., Chem. Commun.*, 1973, 629-630.
39 J. Hartwig, *Organotransition Metal Chemistry: From Bonding to Catalysis*, University Science Books: Sausalito, CA. 2010.
40 M. J. G. Lesley, N. C. Norman, C. R. Rice, D. L. Reger, C. A. Little, J. J. S. Lamba, K. J. Brown, J. C. Peters, J. C. Thomas, S. Sahasrabudhe, et al., Main Group Compounds. *Inorg. Synth.*, 2004, **34**, 1−48.
41 T. J. Del Castillo, N. B. Thompson, and J. C. Peters, *J. Am. Chem. Soc.*, 2016, **138**, 5341−5350.
42 G. R. Fulmer, A. J. M. Miller, N. H. Sherden, H. E. Gottlieb, A. Nudelman, B. M. Stoltz, J. E. Bercaw, and K. I. Goldberg, *Organometallics*, 2010, **29**, 2176−2179.
43 O. V. Dolomanov, L. J. Bourhis, R. J. Gildea, J. A. K. Howard, and H. Puschmann, *J. Appl. Crystallogr.* 2009, **42**, 339-341.
44 G. Sheldrick, *Acta Crystallogr. Sect. A* 2008**, 64**, 112-122.